Reconstructing Permittivity Profiles Using Integral Transforms and Improved Renormalization Techniques

M. J. Akhtar, *Student Member, IEEE,* and Abbas S. Omar, *Senior Member, IEEE*

***Abstract*—Some new ideas for reconstructing permittivity profiles in planar and cylindrical objects illuminated by TEM-, TE- or TM-polarized waves are presented in this paper. For a planar medium, an improved renormalization technique along with a revised version of the nonlinear Riccati differential equation describing the direct problem are introduced. A nonlinear Riccati-similar differential equation for the cylindrical case has also been derived here for the first time, which helps reconstructing radially varying permittivity profiles in a way parallel to that of the planar case. The above-mentioned renormalization technique has been used for the cylindrical case as well to solve the inverse problem making use of a Hankel transform. The method represents fundamental bases for a three-dimensional generalization, which is essential for microwave imaging used, e.g., in biomedical applications and for the diagnostic of diseases in trees and vegetation. A known permittivity profile has been taken to generate synthetic reflection-coefficient data by solving the nonlinear equations describing the direct problems using MATLAB. These data have been used in conjunction with the proposed technique to reconstruct the permittivity profile. About 50–100 data points over the wavelength range from a minimum value (ranging from one-tenth to one-fifth of a typical length in the structure) to infinity have been used for the reconstruction. Reconstructed profiles have been compared to the original ones for a number of cases. Deviations of less than 2% have been achieved.**

***Index Terms*—Electromagnetic scattering, inverse problems, microwave imaging, permittivity, remote sensing.**

I. Introduction

RECONSTRUCTION of permittivity profiles in planar and cylindrical structures constitutes a major part of the electromagnetic inverse scattering and has been of great interest for many years because of many practical applications. It represents the one-dimensional version of the general three-dimensional (3-D) microwave imaging problems needed, for example, for biomedical tomography, which includes reconstruction of muscles, tissues, and different organs of a human being within a microwave imaging process [1]–[5]. Potential areas of radially varying permittivity profiles also include, for example, environmental studies of water content, aging, and possible diseases of trees in forests [6]–[8] and geological investigations of the earth structure as being seen from an exploration well in oil fields [9]. The overall reconstruction process, in general, involves the measurement of scattering data such as the reflection coefficient of an illuminating wave with known characteristics. Information about the unknown permittivity profile of the illuminated object in terms of these measured values is obtained by using some inverse techniques. Different approaches to find out an unknown permittivity profile have been reported. However, most of these methods depend mainly on a source reconstruction philosophy in either the spectral or spatial domain, which leads to a strong nonlinearity inherently connected with nonuniqueness and uncertainty of the achieved solution (see, e.g., [3], [9]–[12]). Only if the so-called "Born approximation" is used, a linear problem with a unique solution can be obtained [13], [14]. This approximation limits the validity of such reconstructions to objects with very low permittivity, which, in practice, are rarely encountered. Recently, the microwave networking technique in conjunction with renormalization methods was used to solve these inverse problems and it was shown that these techniques could be used under both weak and strong scattering conditions [15]–[17]. The main advantage of this method is its "quasi"-linearity, which can lead to a unique solution.

This paper consists of two parts. In the first part, a planar half-space or slab-shaped medium is considered for the detailed analysis. The nonlinear Riccati differential equations for the direct scattering of TEM-, TE-, and TM-polarized illuminations have been formulated in a unified form. This can be used for free space as well as for transmission line and waveguide scattering. The nonlinear renormalization technique presented in [16] and [18] has then been revised to separate the nonlinearity of the corresponding inverse problem into an auxiliary linear differential equation describing a virtual reflection coefficient along with a nonlinear algebraic transformation. The auxiliary equation can then be inverted to get the permittivity profile in terms of an inverse Fourier transform in conjunction with a newly proposed numerical algorithm, which is more appropriate for discrete values of reflection coefficient data. The above-mentioned nonlinear transformation, which transforms the actual measurable reflection coefficient into a virtual one, can be adjusted in order to achieve the required reconstruction accuracy.

In the second part of this paper, we have considered radially varying permittivity profiles in cylindrical structures. A new method has been proposed to reconstruct the profiles in these kind of structures, which goes parallel to the above-mentioned technique for planar mediums. A nonlinear Riccati-similar differential equation has been first formulated for an appropriately defined reflection coefficient. The already mentioned renormalization technique has been used as well in order to separate

Manuscript received August 3, 1999.

The authors are with the Chair of Microwave and Communication Engineering, FET-IPE, University of Magdeburg, 39016 Magdeburg, Germany.

Publisher Item Identifier S 0018-9480(00)06539-X.

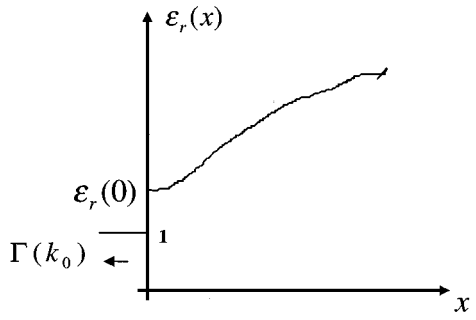

Fig. 1. Half-space medium.

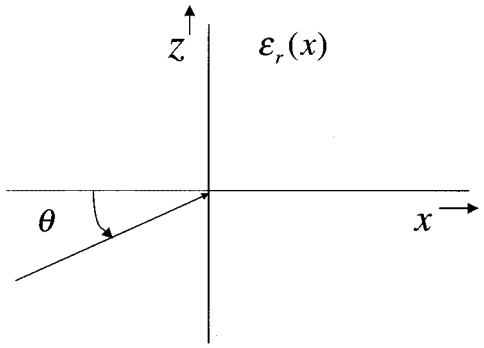

Fig. 2. Reflection at the interface boundary.

the nonlinearity into an algebraic transformation and an auxiliary linear differential equation. The auxiliary equation has then been inverted to get the unknown permittivity profile in terms of a Hankel transform of the virtual reflection coefficient.

II. Planar and Slab-Shaped Geometries

A. Riccati Type Equations for TE-, TM-, and TEM-Polarized Waves

Consider the half-space inhomogeneous medium shown in Fig. 1. The relative permittivity $\varepsilon_r(x)$ is a function of x in the region $x \geq 0$ varying from $\varepsilon_r(0)$ at $x = 0$. This lossless one-dimensional medium can equally represent the filling of a transmission line or waveguide. The exact Riccati differential equation for the reflection coefficient in this type of structures is given by [19]

$$\frac{d\Gamma}{dx} = 2j\beta\Gamma - \frac{1}{2}\left(1-\Gamma^2\right)\frac{d\left(\ln \overline{Z}\right)}{dx} \tag{1}$$

where $\Gamma(x)$ is the local reflection coefficient, $\overline{Z}(x)$ is the normalized local intrinsic impedance, and $\beta(x)$ is the local wavenumber describing propagation in the x-direction. The relationship between $\overline{Z}(x)$, $\beta(x)$ and $\varepsilon_r(x)$ depends, however, on the wave polarization [20] as discussed below.

1) TEM-Polarized Wave: For this case, a monochromatic plane wave of wavenumber k_0 is normally incident from the left-hand side (LHS) at the interface $x = 0$. The normalized impedance and the x-propagation constant are related to the relative permittivity according to

$$\overline{Z}(x) = \frac{Z(x)}{Z_0} = \frac{1}{\sqrt{\varepsilon_r(x)}} \;\&\; \beta(x) = k_0\sqrt{\varepsilon_r(x)}.$$

Substituting these values in (1) results in

$$\frac{d\Gamma}{dx} = 2jk_0\sqrt{\varepsilon_r(x)}\Gamma + \frac{\left(1-\Gamma^2\right)}{4\varepsilon_r(x)}\frac{d\varepsilon_r(x)}{dx} \tag{2}$$

which is the Riccati type differential equation for a TEM-polarized wave.

2) TE-Polarized Wave: Here, we consider a plane wave of wavenumber k_0 incident from the LHS at an angle θ on the interface boundary $x = 0$, as shown in Fig. 2. The electric field of the incident wave is assumed to be parallel to the interface $x = 0$. We then have

$$\beta_z = k_0 \sin\theta \quad (z\text{-propagation constant is the same in air and dielectric.})$$

The propagation constant and the normalized impedance in the x-direction are given by

$$\beta(x) = k_0\sqrt{\varepsilon_r(x) - \sin^2\theta}$$

and

$$\overline{Z}(x) = \frac{k_0}{\beta(x)} = \frac{1}{\sqrt{\varepsilon_r(x) - \sin^2\theta}}.$$

Substituting these values into (1) results in

$$\frac{d\Gamma}{dx} = 2jk_0\sqrt{\varepsilon_r(x) - \sin^2\theta}\,\Gamma + \frac{\left(1-\Gamma^2\right)}{4\left[\varepsilon_r(x) - \sin^2\theta\right]}\frac{d\varepsilon_r(x)}{dx} \tag{3}$$

which is the Riccati type differential equation for a TE-polarized wave.

3) TM-Polarized Wave: Following the same procedure as above, but with the magnetic field of the incident wave being parallel to the interface $x = 0$, the Riccati equation for the TM polarized wave reads

$$\frac{d\Gamma}{dx} = 2jk_0\sqrt{\varepsilon_r(x) - \sin^2\theta}\,\Gamma + \frac{\left(1-\Gamma^2\right)\left[\varepsilon_r(x) - 2\sin^2\theta\right]}{4\varepsilon_r(x)\left[\varepsilon_r(x) - \sin^2\theta\right]}\frac{d\varepsilon_r(x)}{dx}. \tag{4}$$

It is to be noted here that (2)–(4) are the same as given in [16], although using a different approach.

B. Nonlinear Renormalization of Riccati Equations and the Corresponding Inverse Solution

Let us consider a TEM-polarized wave for a detailed analysis. The same approach can be used, however, for TE and TM cases as well (Both cases reduce to TEM for $\theta = 0$). The exact Riccati equation for a TEM wave (2) will be rewritten as

$$\frac{1}{\left(1-\Gamma^2\right)}\frac{d\Gamma}{dx} = 2jk_0\sqrt{\varepsilon_r(x)}\frac{\Gamma}{\left(1-\Gamma^2\right)} + \frac{1}{4\varepsilon_r(x)}\frac{d\varepsilon_r(x)}{dx}. \tag{5}$$

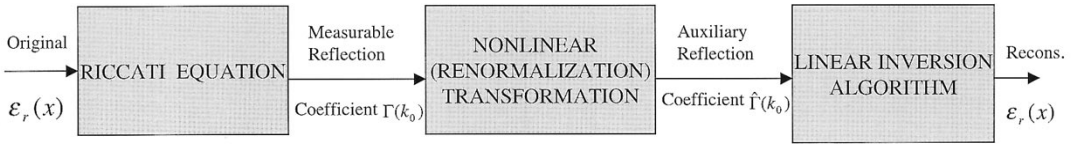

Fig. 3. Schematic diagram for the direct and inverse problems.

We introduce now a virtual reflection coefficient $\hat{\Gamma}$ as the solution of a linearized version of (5), which will be called the auxiliary equation

$$\frac{d\hat{\Gamma}}{dx} = 2jk_0\sqrt{\varepsilon_r(x)}\hat{\Gamma} + \frac{1}{4\varepsilon_r(x)}\frac{d\varepsilon_r(x)}{dx}. \tag{6}$$

Subtracting (5) from (6) results in

$$\left[\frac{d\hat{\Gamma}}{dx} - \frac{1}{(1-\Gamma^2)}\frac{d\Gamma}{dx}\right] = 2jk_0\sqrt{\varepsilon_r(x)}\left[\hat{\Gamma} - \frac{\Gamma}{(1-\Gamma^2)}\right]. \tag{7}$$

Equation (7) would be satisfied exactly irrespective of $\varepsilon_r(x)$ only if

$$\hat{\Gamma} = \tanh^{-1}\Gamma = \frac{\Gamma}{(1-\Gamma^2)} \tag{8}$$

which is not generally true. However, noting that

$$\frac{(1-\Gamma^2)}{\Gamma}\tanh^{-1}(\Gamma) = 1 - \frac{2}{3}\Gamma^2 - \cdots \tag{9}$$

then (8) will be approximately satisfied only when all terms starting by the second one in the right-hand side (RHS) of (9) are negligible. It is then clear that (7) can never be made exactly satisfied. However, it can be approximated in the following two ways: 1) $\hat{\Gamma} = \tanh^{-1}\Gamma$: in this case, only the LHS of (7) will be exactly zero, while the RHS has to be negligible and 2) $\hat{\Gamma} = \Gamma/(1-\Gamma^2)$: in this case, only the RHS of (7) becomes exactly zero, while the LHS has to be negligible.

Generally, all contributions addressed to this problem (e.g., [16], [18]) have taken the first approximation to obtain $\hat{\Gamma}$ from Γ, which is, in fact, biased toward one direction. The other possibility would be to relate $\hat{\Gamma}$ and Γ as in 2), but this is again biased in the other direction. The above approximation can be arbitrarily improved if we look for some optimal function that relates $\hat{\Gamma}$ to Γ. An obvious choice would be to compromise between 1) and 2) or, in other words, to take, for example, the average of both, i.e.,

$$\hat{\Gamma} = \frac{1}{2}\left[\tanh^{-1}\Gamma + \frac{\Gamma}{(1-\Gamma^2)}\right]. \tag{10}$$

In fact, we have found that the above choice is very close to optimum and gives us much better results than that of [16] and [18] for all cases of practical importance. Another alternative can be achieved by inserting (9) in (10) and neglecting the powers of Γ higher than the third

$$\hat{\Gamma} = \frac{\Gamma}{(1-\Gamma^2)} - \frac{1}{3}\Gamma^3. \tag{11}$$

Equation (11) is a good approximation of (10) and can be used to relate $\hat{\Gamma}$ and Γ as well. This is advantageous, especially for the case when the reflection coefficient is given as an analytical function of the wavenumber.

The advantage of the above suggested technique is that we separate the nonlinearity of the exact Riccati equation into a nonlinear algebraic transformation, which relates the actual measurable reflection coefficient Γ to a virtual, not directly measurable, one, i.e., $\hat{\Gamma}$, rendering the differential equation relating $\hat{\Gamma}$ to the looked for permittivity profile linear. This can be visualized as shown in Fig. 3. It is worthy noting that the proposed technique is based on compensating the difference between the original nonlinear Riccati equation (5) and the auxiliary linear one (6) via a nonlinear transformation [e.g., (10)]. There are, in fact, no severe constraints on the choice of the virtual reflection coefficient and the related auxiliary linear differential equation. The choice made by (6) as being a linearization of (5) by neglecting the quadrature term is just one possibility. Other choices are possible as long as a proper transformation between the measurable and virtual reflection coefficients can be found.

Equation (6) is a linear equation in $\hat{\Gamma}$ and, hence, can be inverted for the permittivity profile [17]

$$\varepsilon_r(t) = \varepsilon_r(0)\exp\left[-4\int_0^t \hat{r}_0(t')\,dt'\right] \tag{12}$$

where $\hat{r}_0(t)$ is the Fourier transform of $\hat{\Gamma}_0(k_0)$, which is the virtual reflection coefficient corresponding to $\Gamma_0(k_0)$ given by

$$\Gamma_0(k_0) = \frac{\Gamma(k_0) - R_{01}}{1 - R_{01}\Gamma(k_0)} \tag{13}$$

and

$$t = 2\int_0^x \sqrt{\varepsilon_r(x')}\,dx'. \tag{14}$$

The bilinear transformation in (13) accounts for a jump at $x = 0$ from unity to $\varepsilon_r(0)$. R_{01} can be found graphically in terms of the circle representing the reflection coefficient in the complex plane [21]. The value of $\varepsilon_r(0)$ can be found in terms of the so measured R_{01}, as given in [17].

C. Numerical Algorithm for Reconstructing the Permittivity Profile

Equation (12) gives the permittivity profile $\varepsilon_r(t)$in a virtual time domain. However, to reconstruct the permittivity profile completely, we need to convert it into the space domain. Thus, our main task is to accurately find the value of "x," which corresponds to the particular value of "t." Below we present a simple numerical algorithm based on (14) for this purpose.

Let

$$g(t) = -4\int_0^t \hat{r}_0(t')\,dt' \tag{15}$$

then (12) becomes

$$\varepsilon_r(t) = \varepsilon_r(0)\,\exp\big[g(t)\big]. \tag{16}$$

Starting with $g(0) = 0$, let us follow the development of $g(t)$in time steps Δt. We adopt a simple trapezoidal integration routine described as follows.

1) When $x = 0$, $t = 0$ [according to (14)].
2) At $t = t_1 = \Delta t$

$$g(t_1) = -2\Delta t\big[\hat{r}_0(0) + \hat{r}_0(\Delta t)\big]$$
$$\varepsilon_r(t_1) = \varepsilon_r(0)\,\exp\big[g(t_1)\big].$$

Now, if t_1 corresponds to x_1 via (14), then following the same simple trapezoidal integration algorithm, one arrives at

$$x_1 = \frac{\Delta t}{\Big[\sqrt{\varepsilon_r(0)} + \sqrt{\varepsilon_r(t_1)}\Big]}.$$

3) In general, at $t = t_n = n\Delta t$

$$g(t_n) = g(t_{n-1}) - 2\Delta t\Big\{\hat{r}_0\big[(n-1)\Delta t\big] + \hat{r}_0[n\Delta t]\Big\} \tag{17}$$

$$\varepsilon_r(t_n) = \varepsilon_r(0)\,\exp\big[g(t_n)\big] \tag{18}$$

$$x_n = x_{n-1} + \frac{\Delta t}{\Big[\sqrt{\varepsilon_r(t_{n-1})} + \sqrt{\varepsilon_r(t_n)}\Big]} \tag{19}$$

where t_n corresponds to x_n.

Compared to the algorithm proposed in [17], the algorithm presented here is much more suitable for discrete values of the reflection coefficient. This applies especially when we do the measurement at a number of frequencies and then use the fast Fourier transform (FFT) algorithm to find out the inverse Fourier transform in the virtual "t" domain. The reason is that we get discrete values of the reflection coefficient in the "t" domain at some fixed values of "t" and, hence, it is convenient to take small increments in "t" rather than in "x." Secondly, our algorithm does not assume any approximation as compared to [17] where $\varepsilon_r(x)$ was initially considered to be the same at two different points x_1 and x_2.

D. Reconstruction Examples

We first consider an analytical example, where the reflection coefficient is given by the one-pole expression

$$\Gamma(k_0) = \frac{1}{(1 + j2k_0)}. \tag{20}$$

For this case, $R_{01} = 0$, as was shown in [17] and, hence, $\Gamma_0(k_0) = \Gamma(k_0)$ [from (13)]. If we use the transformation in (11) along with (12), we arrive at

$$\varepsilon_r(t) = \exp\left\{-1\left(1 + t - e^{-t}\right) + \frac{1}{12} \cdot \left[e^{-t/2}\left(-2t^2 - 8t - 16\right) + 16\right]\right\}. \tag{21}$$

The permittivity profile can then be completely reconstructed in the space domain using (21) and the numerical algorithm described above. The exact permittivity profile for this case is well known and is given by [18]

$$\varepsilon_r(x) = (1 + 3x)^{-(4/3)}. \tag{22}$$

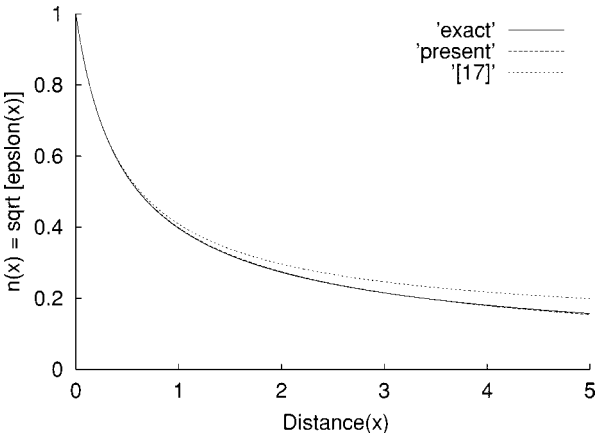

Fig. 4. Exact and reconstructed profiles for the analytical case.

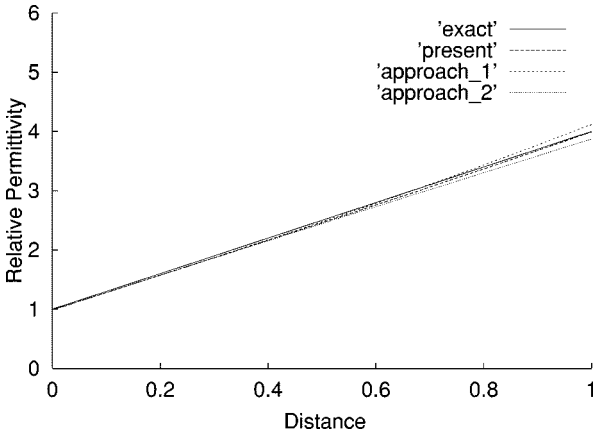

Fig. 5. Exact and reconstructed profiles using different approaches.

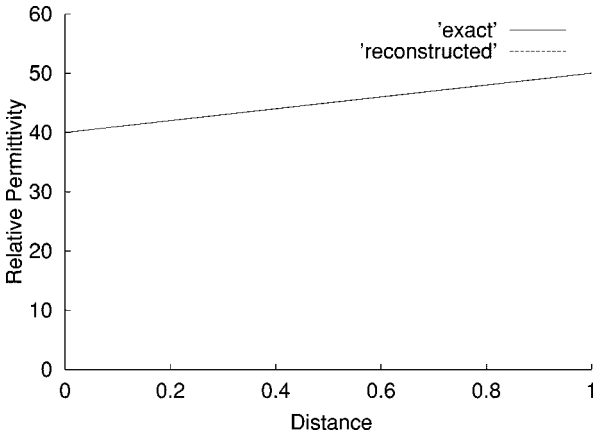

Fig. 6. Exact and reconstructed profiles for a linear case.

Fig. 4 shows a comparison between this exact profile and reconstructed profiles using our present approach and that of [17]. As may be easily seen from these curves, there is a very good agreement between the original and reconstructed profiles using our proposed technique.

Next, we consider linearly varied permittivity profiles. Fig. 5 shows the exact and reconstructed profiles using our proposed method ("present"), "approach_1" using the nonlinear transformation $\hat{\Gamma} = \Gamma/(1 - \Gamma^2)$, and "approach_2" using $\hat{\Gamma} = \tanh^{-1}\Gamma$, i.e., that of [16] or [18]. As may be seen from the

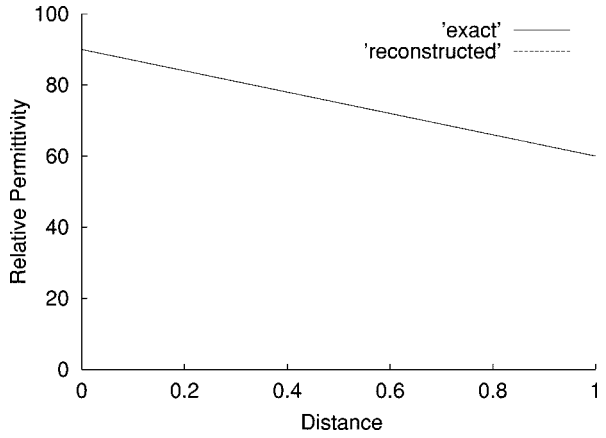

Fig. 7. Exact and reconstructed profiles for quite a high value of permittivity.

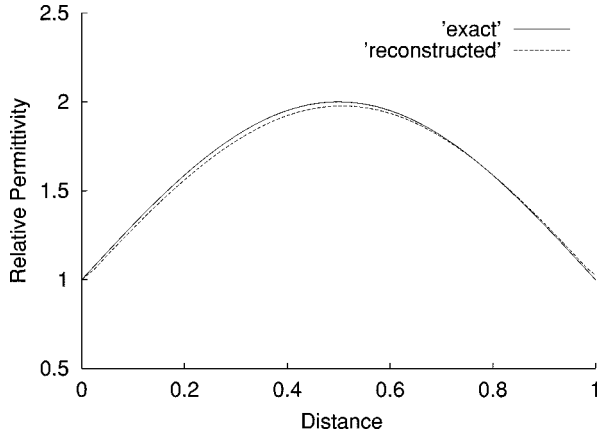

Fig. 8. Exact and reconstructed profiles for a nonlinear case.

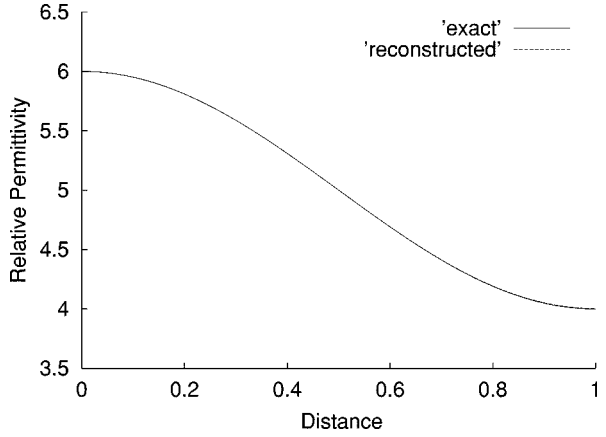

Fig. 9. Exact and reconstructed profiles for a nonlinear case with discontinuity at the air–dielectric interface.

different curves, there is a much better agreement between the exact and reconstructed profiles using our proposed approach and transform as compared to the other two methods. Figs. 6 and 7 show two more linearly varied examples with a quite high relative permittivity and a discontinuity at the air–dielectric interface. As can be seen from these plots, our method works well even when the relative permittivity is as high as 100. Figs. 8 and 9 show nonlinear cases, which contain more contrast in the

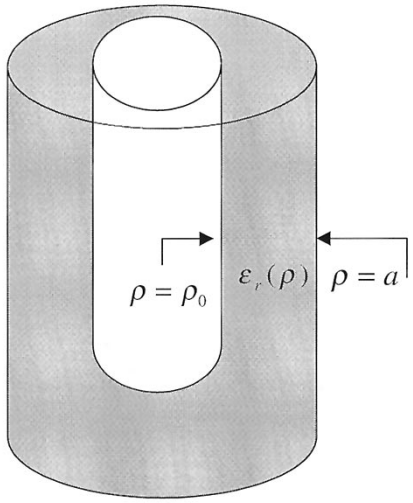

Fig. 10. Radially varying permittivity profile.

permittivity profile. Again, an excellent agreement between the original and reconstructed profiles has been achieved.

In all numerical examples mentioned above, the exact nonlinear Riccati equation was first solved using MATLAB for the given permittivity profile to simulate reflection-coefficient measurement data, which means error- and noise-free measurements. These values were then used in our proposed algorithm to reconstruct the profiles. Although 100 data points were used for reconstruction in the above examples, as few as 50 data points covering the spectral wavelength range from infinity down to one-tenth of the maximum depth, over which the permittivity changes, were enough to achieve a reconstruction accuracy of 2%. In all plots, the distance has been normalized with respect to the maximum depth over which the permittivity is to be reconstructed. We also considered many other profiles for validation of our algorithm with and without permittivity jumps at the air–dielectric interfaces. All have shown similar reconstruction-accuracy behavior.

III. Cylindrical Structures

A. Derivation of the Riccati-Similar Differential Equation

Consider the cylindrical dielectric object with a radially dependent permittivity $\varepsilon_r(\rho)$ shown in Fig. 10. A monochromatic cylindrical wave of wavenumber k_0 is assumed to be incident from the outer free space, ($\rho > a$). This accounts, in fact, to the case of outside illuminations as, for example, in the investigation of trees and biological bodies. It is readily proven that illuminating cylindrical waves with different azimuthal and axial dependences are decoupled. Without a considerable loss of generality, we will consider the TM_{00} illumination (see, e.g., [20]), which represents an axially and azimuthally independent incident wave. The analysis of other illuminations is principally similar, except for the frequency dependence of their radial propagation constants, which has to be differently treated. The TM_{00} mode in a radial waveguide or a cylindrical structure is similar to the TEM mode in transmission lines, as it neither has E- nor H-field components in the direction of propagation (ρ-direction) [20]. As we measure the reflection coefficient at

the outer radius of the cylindrical body, thus we will consider the inward and outward traveling waves as being incident and reflected ones, respectively. For a TM_{00} mode, we have

$$E_z^- = -j\omega\mu_0 H_0^{(1)}(k\rho) \quad H_\phi^- = k_0\sqrt{\varepsilon_r(\rho)}H_1^{(1)}(k\rho) \tag{23}$$

$$E_z^+ = -j\omega\mu_0 H_0^{(2)}(k\rho) \quad H_\phi^+ = k_0\sqrt{\varepsilon_r(\rho)}H_1^{(2)}(k\rho) \tag{24}$$

where "$-$" and "$+$" signs represent inward and outward propagating waves, respectively, $H_m^{(n)}(k\rho)$ represents a Hankel function of an nth type and mth order, and

$$k = k_0\sqrt{\varepsilon_r(\rho)}. \tag{25}$$

Let us now look for a taper solution of the form

$$E_z = E_z^- + \tilde{\Gamma}E_z^+ = E_z^- - \tilde{\Gamma}\left(E_z^-\right)^* \tag{26}$$

$$H_\phi = H_\phi^- + \tilde{\Gamma}H_\phi^+ = H_\phi^- + \tilde{\Gamma}\left(H_\phi^-\right)^* \tag{27}$$

where $\tilde{\Gamma}$ is an appropriately defined reflection coefficient and "*" represents the complex conjugate.

Let us also define

$$Y = \frac{H_\phi^-}{E_z^-} = jY_0\sqrt{\varepsilon_r(\rho)}\,\frac{H_1^{(1)}(k\rho)}{H_0^{(1)}(k\rho)} \tag{28}$$

and

$$\alpha = \frac{Y^*}{Y} = -\frac{H_0^{(1)}(k\rho)H_1^{(2)}(k\rho)}{H_0^{(2)}(k\rho)H_1^{(1)}(k\rho)} \tag{29}$$

where Y_0 is the free-space intrinsic admittance.

After some mathematical manipulations of (26)–(29), we arrive at

$$\begin{aligned} E_z &= E_z^-(1+\Gamma) \\ H_\phi &= YE_z^-(1-\alpha\Gamma) \end{aligned} \tag{30}$$

where

$$\Gamma = -\tilde{\Gamma}\,\frac{(E_z^-)^*}{E_z^-}. \tag{31}$$

Now, for a TM_{00} mode, Maxwell's equations are reduced to

$$\begin{aligned} j\omega\mu_0 H_\phi &= \frac{\partial E_z}{\partial\rho} \\ jk_0Y_0\varepsilon_r(\rho)\rho E_z &= \frac{\partial}{\partial\rho}(\rho H_\phi). \end{aligned} \tag{32}$$

From (30) and (32), we get

$$jk_0\overline{Y}(1-\alpha\Gamma)E_z^- = \frac{\partial}{\partial\rho}\left[E_z^-(1+\Gamma)\right] \tag{33}$$

$$jk_0\varepsilon_r(\rho)\rho E_z^-(1+\Gamma) = \frac{\partial}{\partial\rho}\left[\rho\overline{Y}(1-\alpha\Gamma)E_z^-\right] \tag{34}$$

where

$$\overline{Y} = \frac{Y}{Y_0} = j\sqrt{\varepsilon_r(\rho)}\,\frac{H_1^{(1)}(k\rho)}{H_0^{(1)}(k\rho)} \tag{35}$$

is the local normalized admittance. Eliminating E_z^-, one arrives at the following nonlinear differential equation for Γ

$$\begin{aligned} &\frac{d\Gamma}{d\rho} + \frac{jk_0}{(1+\alpha)\overline{Y}}\left[\varepsilon_r(\rho)(1+\Gamma)^2 - \overline{Y}^2(1-\alpha\Gamma)^2\right] \\ &\quad + \frac{(1+\Gamma)}{(1+\alpha)\rho\overline{Y}}\left[\frac{d\alpha}{d\rho}\Gamma\rho\overline{Y} + (\alpha\Gamma-1)\,\frac{\partial}{\partial\rho}\left(\rho\overline{Y}\right)\right] \\ &\quad = 0. \end{aligned} \tag{36}$$

In order to have a Riccati-similar fashion, we rewrite (36) in the following form:

$$\begin{aligned} &\frac{d\Gamma}{d\rho} + \Gamma\left[\frac{4j}{\pi\rho H_0^{(1)}(k\rho)H_0^{(2)}(k\rho)} - \frac{j\pi k_0\rho}{8\sqrt{\varepsilon_r(\rho)}}\right. \\ &\qquad \left.\cdot\left(H_0^{(1)}(k\rho)H_1^{(2)}(k\rho) + H_1^{(1)}(k\rho)H_0^{(2)}(k\rho)\right)\frac{d\varepsilon_r(\rho)}{d\rho}\right] \\ &\quad = \frac{j\pi k_0\rho}{8\sqrt{\varepsilon_r(\rho)}}\,\frac{d\varepsilon_r(\rho)}{d\rho}\,H_1^{(1)}(k\rho)H_0^{(2)}(k\rho)\left[1-\alpha\Gamma^2\right] \end{aligned} \tag{37}$$

which is a nonlinear Riccati-similar differential equation for the radially (and frequency) dependent reflection coefficient $\Gamma(k_0, \rho)$ due to TM_{00} illumination.

B. Inversion of the Radially Dependent Permittivity Profile

For most practical cases considered, "α," as defined in (29), can be replaced by its asymptotic value for $k\rho \to \infty$. Hence, (37) can be rewritten as

$$\begin{aligned} &\frac{1}{(1-\Gamma^2)}\,\frac{d\Gamma}{d\rho} + \frac{\Gamma}{(1-\Gamma^2)} \\ &\quad\cdot\left[\frac{4j}{\pi\rho H_0^{(1)}(k\rho)H_0^{(2)}(k\rho)} - \frac{j\pi k_0\rho}{8\sqrt{\varepsilon_r(\rho)}}\right. \\ &\qquad\left.\cdot\left(H_0^{(1)}(k\rho)H_1^{(2)}(k\rho) + H_1^{(1)}(k\rho)H_0^{(2)}(k\rho)\right)\frac{d\varepsilon_r(\rho)}{d\rho}\right] \\ &\quad = \frac{j\pi k_0\rho}{8\sqrt{\varepsilon_r(\rho)}}\,\frac{d\varepsilon_r(\rho)}{d\rho}\,H_1^{(1)}(k\rho)H_0^{(2)}(k\rho). \end{aligned} \tag{38}$$

The structural form of (38) now becomes similar to that of (5). Consequently, we can make use of the same renormalization technique as proposed for the planar case. Hence, the measurable reflection coefficient $\Gamma(\rho)$ can be related to a virtual one $\hat{\Gamma}(\rho)$ via a nonlinear transformation. Again, the advantage of this procedure is that we isolate the nonlinearity of (38) into a nonlinear algebraic transformation rendering the differential equation describing $\hat{\Gamma}(\rho)$ linear. An appropriate linearized version of (38), which can be used to define $\hat{\Gamma}(\rho)$, is given by

$$\begin{aligned} &\frac{d\hat{\Gamma}}{d\rho} + \hat{\Gamma}\left[\frac{4j}{\pi\rho H_0^{(1)}(k\rho)H_0^{(2)}(k\rho)} - \frac{j\pi k_0\rho}{8\sqrt{\varepsilon_r(\rho)}}\right. \\ &\qquad\left.\cdot\left(H_0^{(1)}(k\rho)H_1^{(2)}(k\rho) + H_1^{(1)}(k\rho)H_0^{(2)}(k\rho)\right)\frac{d\varepsilon_r(\rho)}{d\rho}\right] \\ &\quad = \frac{j\pi k_0\rho}{8\sqrt{\varepsilon_r(\rho)}}\,\frac{d\varepsilon_r(\rho)}{d\rho}\,H_1^{(1)}(k\rho)H_0^{(2)}(k\rho). \end{aligned} \tag{39}$$

We will take the same optimum nonlinear transformation defined by (10) to relate $\Gamma(\rho)$ and $\hat{\Gamma}(\rho)$, as described earlier for the planar case. Making use of some simplifying assumptions, (39) can be approximated to

$$\frac{d\hat{\Gamma}}{d\rho}+\hat{\Gamma}\left[k\,\frac{H_0^{(1)^2}(k\rho)-H_1^{(1)^2}(k\rho)}{H_0^{(1)}(k\rho)H_1^{(1)}(k\rho)}\right]=\frac{j}{4\varepsilon_r(\rho)}\,\frac{d\varepsilon_r(\rho)}{d\rho}\cdot\frac{H_1^{(1)}(k\rho)}{H_0^{(1)}(k\rho)}. \quad (40)$$

In order to justify the practical equivalence between (39) and (40), both have been solved numerically for a variety of permittivity profiles to get $\hat{\Gamma}(\rho)$. It was found that there is a very close proximity between the values of $\hat{\Gamma}(\rho)$ as given by these two equations for almost all practical cases. Integrating (40) with boundary condition $\hat{\Gamma}(k_0, \rho_0) = 0$ results in

$$\hat{R}(k_0) = \hat{\Gamma}(k_0, a) = \int_a^{\rho_0} \frac{j\pi k\rho'}{8\varepsilon_r(\rho')}\,\frac{d\varepsilon_r(\rho')}{d\rho'}\,H_1^{(1)^2}(k\rho')\,\exp(-j2ka)\,d\rho' \quad (41)$$

where "a" and "ρ_0" are the outer and inner radii of the cylindrical object under consideration, respectively, as shown in Fig. 10. A further processing of (41) necessitates that "k" be ρ independent, which is not the case [see (25)]. As a simplification, which has to be justified later, the following two approximations for "k" have been considered:

- $k = k_0$;
- $k = k_0 c$, where "c" is a constant depending on the relative permittivity at the two ends.

We have solved the inverse problem using both approaches, as given in one of the examples. We have observed that a good approximation for "c^2" is the average value of the permittivity at both ends, i.e.,

$$k = k_0\sqrt{\frac{\varepsilon_r(a)+\varepsilon_r(\rho_0)}{2}}. \quad (42)$$

The advantage of having ρ-independent "k" is to isolate the terms containing $\varepsilon_r(\rho')$ in (41) and, hence, to simplify the overall inversion process as will be shown below. Now, going parallel to the planar geometry, we first find the truncated Hankel transform of $\hat{R}(k_0)$, which is the natural one in cylindrical coordinate systems

$$\hat{r}(\rho) = \int_0^{\hat{k}} \hat{R}(k_0)\,J_0(k\rho)k\,dk \quad (43)$$

where "$\hat{k}$" is the highest wavenumber corresponding to "$\hat{k}_0$" according to (42) at which the reflection coefficient is to be measured. It is readily proven that $\hat{r}(\rho)$ is related to $\varepsilon_r(\rho)$ by

$$\hat{r}(\rho) = \int_a^{\rho_0} G(\varepsilon_r(\rho'))\,K(\rho, \rho')\,\rho'\,d\rho' \quad (44)$$

where

$$G(\varepsilon_r(\rho')) = \frac{\pi}{8\varepsilon_r(\rho')}\,\frac{d\varepsilon_r(\rho')}{d\rho'} \quad (45)$$

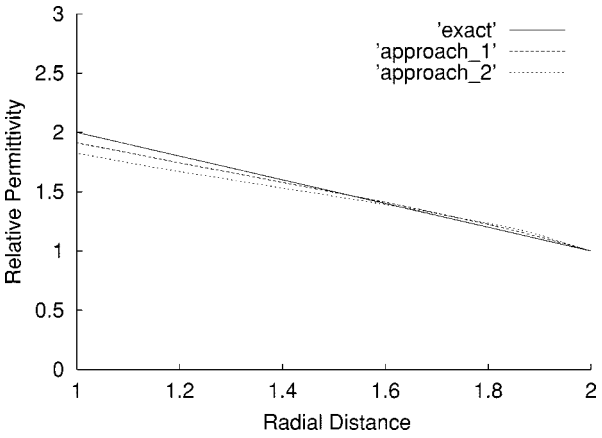

Fig. 11. Exact and reconstructed profiles using two approaches in the cylindrical geometry.

and

$$K(\rho, \rho') = \int_0^{\hat{k}} jkH_1^{(1)^2}(k\rho')\,\exp(-j2ka)J_0(k\rho)k\,dk. \quad (46)$$

The function $K(\rho, \rho')$ defined by (46) is, in fact, a variable-resolution selective function with a maximum at $\rho' = \hat{\rho}(\rho)$. It can be used to sample $G(\varepsilon_r(\rho'))$ at $\rho' = \hat{\rho}$ according to

$$G\big(\varepsilon_r(\hat{\rho})\big) = \frac{\hat{r}\big(\rho(\hat{\rho})\big)}{\int_a^{\rho_0} K\big(\rho(\hat{\rho}), \rho'\big)\rho'\,d\rho'} \quad (47)$$

where $\rho(\hat{\rho})$ is the inverse function of $\hat{\rho}(\rho)$.

A higher resolution of the construction is obtained by increasing $\hat{k}$. Finally, the unknown permittivity profile $\varepsilon_r(\rho')$ can be easily reconstructed using (45)

$$\varepsilon_r(\rho') = \varepsilon_r(a)\,\exp\left[\frac{8}{\pi}\int_a^{\rho'} G(\varepsilon_r(x))\,dx\right] \quad (48)$$

where $\varepsilon_r(a)$ is the permittivity at the outer air–dielectric interface and x is a dummy integration variable.

It is worth noting that practical antenna arrangements for illumination (transmitters) or measurement of scattering data (receivers) are not generally able to excite or measure a single radial mode (e.g., TM_{00}). An arbitrary illuminating or scattered electromagnetic field can, however, be expanded into an infinite sum of radial modes due to their completeness property (see, e.g., [22]). A multiple illumination/multiview scenario can then be used to extract the necessary information on the scattering of a certain radial mode. The above-mentioned issue is not, however, our concern in this paper, as the scattering data used for the verification of the proposed method have been synthetically produced by solving the direct problem for known permittivity profiles.

C. Reconstruction Examples

Fig. 11 shows the exact and reconstructed permittivity profiles for the case, when the relative permittivity at the outer radius is continuous (jump free) using two different approaches. In the first approach, the value of "k" is taken as given by (42) for the solution of the inverse problem. In the second approach, the value of "k" is simply taken equal to "k_0." As expected, the first

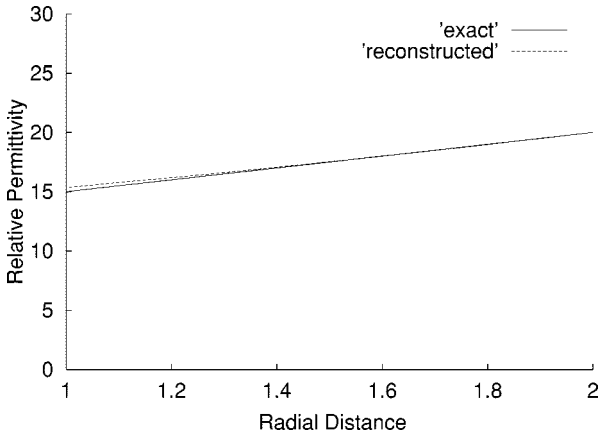

Fig. 12. Exact and reconstructed profiles with discontinuity at the air–dielectric interface in the cylindrical geometry.

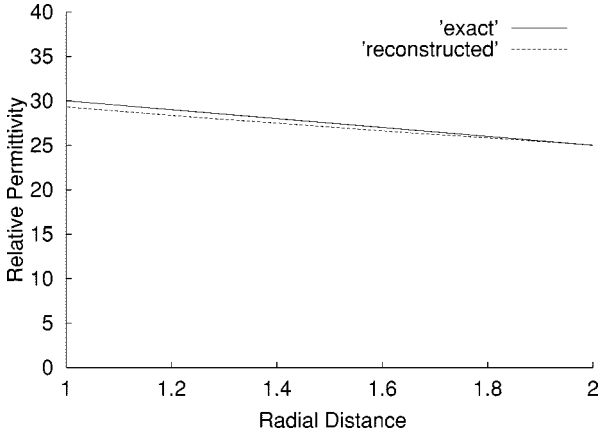

Fig. 13. Exact and reconstructed profiles for a high value of permittivity in the cylindrical geometry.

approach gives quite good matching between actual and reconstructed profiles as compared to the second one. Thus, the first approach will be adopted for the considered examples. Figs. 12 and 13 show the exact and reconstructed profiles, when the relative permittivity is quite high. As can be easily seen, the agreement between exact and reconstructed profiles is quite good, especially for higher values of permittivity. As in the planar case, error- and noise-free scattering data have been synthetically produced by solving the nonlinear Riccati-similar differential equation (38) for known permittivity profiles using MATLAB. As few as 50 data points covering the spectral wavelength range from infinity down to one-fifth of the inner diameter of the cylindrical object have been used for the reconstruction. The radial distance in the above plots has been normalized with respect to the inner radius of the cylindrical object under consideration. Effects of noisy results are being considered.

IV. Conclusion

We have presented some new ideas for reconstructing the permittivity profiles in both planar and cylindrical geometries. An improved renormalization technique has been proposed for the solution of the inverse problems, which can be equally used for both cases. A practically unique solution can be obtained using our proposed method as it isolates the nonlinearity associated with the inverse problems into a simple algebraic transformation. On the other hand, the method is not based on a Born approximation and, hence, can be used to reconstruct profiles with higher contrasts as well. Several examples have been considered for validation of the proposed technique and, in each case, a quite good agreement has been found between the original and reconstructed profiles. Lossy profiles related to vegetation and biological bodies are currently being considered for analysis.

References

[1] D. K. Ghodgaonkar, O. P. Gandhi, and M. J. Hagmann, "Estimation of complex permittivities of a three-dimensional inhomogeneous biological bodies," *IEEE Trans. Microwave Theory Tech.*, vol. MTT-31, pp. 442–446, June 1983.

[2] A. Broquetas, J. Romeu, J. M. Rius, A. R. Elias-Fuste, A. Cardama, and L. Jofre, "Cylindrical geometry: A further step in active microwave tomography," *IEEE Trans. Microwave Theory Tech.*, vol. 39, pp. 836–844, May 1991.

[3] N. Joachimowicz, J. J. Mallorqui, J.-C. Bolomey, and A. Broquetas, "Convergence and stability assessment of Newton–Kantorovich reconstruction algorithm for microwave tomography," *IEEE Trans. Med. Imag.*, vol. 17, pp. 562–570, Aug. 1998.

[4] N. Joachimowicz, C. Pichot, and J.-P. Hugonin, "Inverse scattering: An iterative numerical method for electromagnetic imaging," *IEEE Trans. Antennas Propagat.*, vol. 39, pp. 1743–1752, Dec. 1991.

[5] S. Caorsi, G. L. Gragnani, and M. Pastorino, "Reconstruction of dielectric permittivity distributions in arbitrary 2-D inhomogeneous biological bodies by a multiview microwave numerical method," *IEEE Trans. Med. Imag.*, vol. 12, pp. 232–239, June 1993.

[6] L. Tsang and J. A. Kong, "Application of strong fluctuation random medium theory to scattering from vegetation-like half space," *IEEE Trans. Geosci. Remote Sensing*, vol. GRS-19, pp. 62–69, 1981.

[7] M. O. Kolawole, "Scattering from dielectric cylinders having radially layered permittivity," *J. Electromag. Waves Applicat.*, vol. 6, pp. 235–259, 1992.

[8] M. A. Karam, A. K. Fung, and Y. M. M. Antar, "Electromagnetic wave scattering from some vegetation samples," *IEEE Trans. Geosci. Remote Sensing*, vol. 26, pp. 799–807, Nov. 1988.

[9] T. M. Habashy and R. Mittra, "Review of some inverse methods in electromagnetics," *J. Opt. Soc. Amer. A, Opt. Image Sci.*, vol. 4, pp. 281–291, Jan. 1987.

[10] J. J. Xia, T. M. Habashy, and J. A. Kong, "Profile inversion in a cylindrically stratified lossy medium," *Radio Sci.*, vol. 29, pp. 1131–1141, July–Aug. 1994.

[11] T. M. Habashy, W. C. Chew, and E. Y. Chow, "Simultaneous reconstruction of permittivity and conductivity profiles in a radially inhomogeneous slab," *Radio Sci.*, vol. 21, pp. 635–645, July–Aug. 1986.

[12] P. V. Frangos and D. l. Jaggard, "A numerical solution to the Zakharov–Shabat inverse scattering problem," *IEEE Trans. Antennas Propagat.*, vol. 39, pp. 74–79, Jan. 1991.

[13] W. Tabarra, "Reconstruction of permittivity profiles from a spectral analysis of the reflection coefficient," *IEEE Trans. Antennas Propagat.*, vol. AP-27, pp. 241–248, Mar. 1979.

[14] A. K. Jordan and H. D. Ladouceur, "Renormalization of an inverse-scattering theory for discontinuous profiles," *Phys. Rev. A, Gen. Phys.*, vol. 36, p. 4245, 1987.

[15] T. J. Cui and C. H. Liang, "Reconstruction of the permittivity profile of an inhomogeneous medium using an equivalent network method," *IEEE Trans. Antennas Propagat.*, vol. 41, pp. 1719–1726, Dec. 1993.

[16] ——, "Nonlinear differential equation for the reflection coefficient of an inhomogeneous lossy medium and its inverse scattering solutions," *IEEE Trans. Antennas Propagat.*, vol. 42, pp. 621–626, May 1994.

[17] ——, "Novel applications of an approximate profile inversion for one-dimensional medium," *IEEE Trans. Antennas Propagat.*, vol. 43, pp. 308–312, Mar. 1995.

[18] D. L. Jaggard and Y. Kim, "Accurate one-dimensional inverse scattering using a nonlinear renormalization technique," *J. Opt. Soc. Amer. A, Opt. Image Sci.*, vol. 2, pp. 1922–1930, Nov. 1985.

[19] R. E. Collin, *Foundation for Microwave Engineering*. New York: McGraw-Hill, 1966.

[20] R. F. Harrington, *Time-Harmonic Electromagnetic Fields*. New York: McGraw-Hill, 1961.

[21] K. I. Hopcraft and P. R. Smith, "Geometrical properties of backscattered radiation and their relation to inverse scattering," *J. Opt. Soc. Amer. A, Opt. Image Sci.*, vol. 6, pp. 508–516, 1989.
[22] P. Morse and H. Feshbach, *Methods of Theoretical Physics*. New York, NY: McGraw-Hill, 1953.

M. J. Akhtar (S'98) was born in Gaya, India, in March 1971. He received the B.Sc. Engg. degree in electronics engineering from Aligarh Muslim University, Aligarh, India, in 1990, and the M.E. degree in electronics and communication engineering with a specialization in microwave engineering from the Birla Institute of Technology, Ranchi, India, in 1993, and is currently working toward the Ph.D. degree in electrical engineering at the University of Magdeburg, Magdeburg, Germany. His Ph.D. research involves the solution of electromagnetic inverse-scattering problems and its application to the field of remote sensing and microwave imaging

From 1993 to 1994, he was a Research Associate with the Central Electronics Engineering Research Institute, Pilani, India, and since 1993, he has been a Scientist. His research interests include the design and development of microwave tubes, optical control of microwave devices, and numerical techniques applied to the electromagnetic-field problems.

Mr. Akhtar is a member of the Institution of Electronics and Telecommunication Engineers (IETE), New Delhi, India, the Indian Physics Association (IPA), and the Indo–French Technical Association (IFTA).

Abbas S. Omar (M'87–SM'89) received the B.Sc., M.Sc. and Doktor-Ing. degrees in electrical engineering in 1978, 1982, and 1986, respectively.

Since 1990, he has been a Professor of electrical engineering and, since 1998, the Head of Chair of Microwave and Communication Engineering, University of Magdeburg, Magdeburg, Germany. He has authored and co-authored over 130 technical papers extending over a wide spectrum of research areas. He recently directed his search activities to the solution of inverse problems related to remote sensing and microwave tomography. His current research fields cover the areas of remote sensing and microwave imaging, high-speed multimedia satellite and mobile communication, electromagnetic bullets and their applications to secure low-power wide-band communications and subsurface tomography, stochastical electromagnetics and their meteorological, environmental and biomedical applications, field theoretical modeling of microwave systems and components, microwave measurements and submillimeter-wave signal generation, and processing. He is on the Editorial Board of the *Proceeding of the Institution of Electrical Engineers*, *Electronics Letters*, and the *Journal of Electromagnetics*.

Dr. Omar is a member of the Technical Program Committee of the IEEE Microwave Theory and Techniques Society (IEEE MTT-S) Symposium, and is the IEEE MTT-S Financial Coordinator for Region 8. He is on the Editorial Board of the IEEE TRANSACTIONS ON MICROWAVE THEORY AND TECHNIQUES, the IEEE TRANSACTIONS ON ANTENNAS AND PROPAGATION, and IEEE MICROWAVE AND GUIDED WAVE LETTERS.